

Article

Improved Low-Temperature Activity of V_2O_5 - WO_3 / TiO_2 for Denitration Using Different Vanadium Precursors

Lina Gan ^{1,2}, Feng Guo ¹, Jian Yu ^{1,*} and Guangwen Xu ^{1,*}

¹ State Key Laboratory of Multiphase Complex Systems, Institute of Process Engineering, Chinese Academy of Sciences, Beijing 100190, China; lngan@ipe.ac.cn (L.G.); guofeng@ipe.ac.cn (F.G.)

² University of Chinese Academy of Sciences, Beijing 100049, China

* Correspondence: yujian@ipe.ac.cn (J.Y.); gwxu@ipe.ac.cn (G.X.); Tel: +86-10-8254-4886 (J.Y. & G.X.); Fax: +86-10-8262-9912 (J.Y. & G.X.)

Academic Editor: Keith Hohn

Received: 22 December 2015; Accepted: 25 January 2016; Published: 5 February 2016

Abstract: This work tested two V_2O_5 - WO_3 / TiO_2 catalysts with different vanadium precursors for selective catalytic reduction (SCR) of flue gas NO using NH_3 at 150–450 °C. While catalyst A was prepared using ammonium metavanadate (NH_4VO_3) through incipient impregnation, catalyst B was made according to the solvothermal method using vanadyl acetylacetonate ($VO(acac)_2$) as the vanadium precursor. The catalytic evaluation for denitration was in a laboratory fixed bed reactor using simulated flue gas under conditions of a gas hourly space velocity (GHSV) of 40,000 h^{-1} and an NH_3 /NO molar ratio of 0.8. Without SO_2 and water vapor in the flue gas at 200 °C, the realized NO conversion was 56% for catalyst A but 80% for B. The presence of 350 ppm SO_2 and 10 vol. % water vapor in the flue gas slightly reduced the NO conversion over catalyst B, and its activity was stable in a 108-h continuous test at temperatures varying from 450 °C to 220 °C. Via fourier transformation infrared spectroscopy (FT-IR) and thermogravimetric (TG) analysis, it was shown that over catalyst B a dynamic balance between the formation and decomposition of ammonium sulfite or sulfate is built possibly at temperatures as low as 220 °C. For this catalyst there was a higher surface atomic concentration of vanadium and a higher ratio of $V^{4+}/(V^{4+} + V^{5+})$, while the NH_3 adsorption test revealed more acidic sites on catalyst B. The study discloses a potentially new approach to prepare a V_2O_5 - WO_3 / TiO_2 catalyst with good performance for SCR of flue gas NO at 220–300 °C.

Keywords: vanadium precursor; denitration; SCR; low-temperature activity; vanadyl acetylacetonate

1. Introduction

Nitrogen oxides (NO_x) including NO, NO_2 and N_2O remain as one of the major sources of air pollution, which greatly contribute to the greenhouse effect, ozone depletion, and formation of photochemical smog, acid rain, and particulate matters [1]. Many countries have made stringent emission limits for flue gases from combustion facilities and vehicles. For China, the NO_x from stationary combustion including power boilers and industrial furnaces takes about 70% of the total NO_x emission, while this is about 30% from vehicles. The former has been paid much more attention by far to control in the last ten years, making the contribution of vehicles gradually bigger in the actual emission of NO_x into air. The pattern of air pollution in some big cities has been shifting from coal-burning pollution to traffic pollution [2].

The selective catalytic reduction (SCR) of NO_x by NH_3 in the presence of excessive oxygen is a well-proven and widely-applied technology for controlling NO_x from stationary power stations and diesel engines [3–6]. Many efforts have been made in the development of catalyst and reaction

systems for SCR [7–9]. V_2O_5 - WO_3 / TiO_2 and V_2O_5 - MoO_3 / TiO_2 catalysts have been widely used for decades. However, these catalysts are efficient only within a relatively narrow temperature window of 300–400 °C, which could not meet the actual demand for NO_x removal in industrial combustion utilities and city buses with diesel engines. The flue gas exhaust temperatures are usually 150–300 °C for industrial combustion facilities including industrial steam boilers, with two thirds of them above 200 °C [10,11]. Power boilers have also 20% of their working time at low load and start-up or shut-down to exhaust low-temperature flue gas, say at 250–300 °C, before the economizer. For diesel vehicles driving in steady state, the temperature of the exhaust gas is between 180 and 280 °C but it can also reach 440 °C when the engine runs at high speed [12]. By on-road evaluation of the Euro IV vehicle emission factors, Fu *et al.* [13] reported that the NO_x emission factor for urban and suburban driving is higher than that for freeway driving. Their NO_x emission factors are higher than the Euro IV limits because of their low exhaust temperatures. Li *et al.* [14] reported that the State IV transit bus equipped with SCR system has exhaust gas at low temperatures and high NO_x emission. Therefore, it is urgent to explore how to reduce the NO_x emission at low flue gas temperatures at 200 to 400 °C, which has considerable application not only to industrial combustion facilities but also to diesel engines.

Many efforts have been made to develop high-performance low-temperature SCR catalysts. The use of some transition metals has attracted great attention, including Mn, Ce, Cu, Fe, Ag, Pt, Pd, Rh, and Co [15–21]. Qi *et al.* [19–21] found that the Mn-Ce mixed-oxide catalyst yielded nearly 100% NO conversion at 120 °C, and the concentration of N_2O increased with raising the temperature and manganese content. This catalyst was within a narrow temperature window of 100–200 °C but it would be hard to use for flue gases containing SO_2 and water vapor exhaust, for example, from coal-burning facilities and diesel engines. Yu *et al.* [10] verified the non-recoverable deactivation of Mn-base catalyst for the formation of manganese sulfate.

Transition metal acetylacetonate complexes, e.g., $VO(acac)_2$ [22–25], $Cr(acac)_3$ [26], and $Cu(acac)_2$ [27] have been used as support of catalysts or to prepare thin-film catalyst ($acac = acetylacetonate, C_5H_7O_2$). Vanadyl acetylacetonate ($VO(acac)_2$) is shown to be a good vanadium precursor for synthesizing oxovanadium complexes [28–30]. The replacement of an acetylacetonato ligand by bidentate and tridentate chiral ligands provides a way of producing optically actively vanadium complexes, which have been extensively used in asymmetric catalysis. In the liquid phase, $VO(acac)_2$ prefers to bond to a silica surface through a hydrogen bond between the acetylacetonate ring and surface silanols. This causes in turn isolated metal ions on the support surface guaranteeing the high dispersion of active sites [31,32]. In addition, Economidis *et al.* [33] found that the valence of vanadium in the precursor solution plays a very important role in the synthesis of the catalyst, and the reduction of V^{5+} to V^{4+} results in a better-performance catalyst. $VO(acac)_2$ deposited on TiO_2 , TiO_2 - SiO_2 , Al_2O_3 - SiO_2 , and SBA-15 by liquid or gas phase dispersion techniques has been well studied [22–24,34], but there has been little reporting on the use of $VO(acac)_2$ as a vanadium precursor and WO_3 - TiO_2 used as support for the NO reduction catalyst made by the solvothermal method. This work attempts such an idea and is concerned with testing the potential denitration catalyst by the solvothermal preparation method, using $VO(acac)_2$ as the vanadium precursor to realize a wide working-temperature window of, for example, 220–450 °C for NO reduction by NH_3 in flue gases containing SO_2 and water vapor.

2. Results and Discussion

Figure 1a compares the NO conversions realized over the catalysts A to D under similar conditions shown in the experimental section for simulated flue gas without SO_2 and water vapor. Comparing the catalysts A and C, which had the same vanadium precursor NH_4VO_3 but different preparation methods, one can see that there is almost no obvious difference in the realized NO conversion that actually represents the de- NO_x activity of a catalyst. For the catalysts B and D using $VO(acac)_2$ as the vanadium precursor, however, their realized de- NO_x activities are higher than the catalysts A and C based on NH_4VO_3 precursor. Furthermore, the catalyst B manifested the best activity at low temperatures. Therefore, for analyzing the potential improvement on low-temperature activity and

its mechanism by using different precursors, all tests herein were conducted only for the catalysts A and B.

At high GHSV, the diffusion effect is weak so that the reaction is more subject to kinetic control. As shown in Figure 1b, there was obvious difference in activity for the catalysts A and B at GHSV 240,000 h⁻¹.

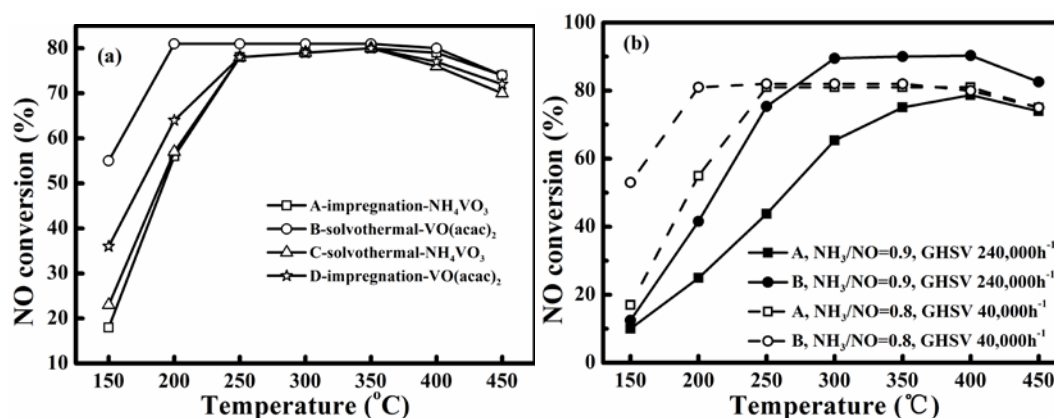


Figure 1. (a) NO conversions of four prepared catalysts A to D for simulated flue gas without SO₂ and water vapor; (b) NO conversion of catalyst A and B under different GHSV: NH₃/NO = 0.8, GHSV 40,000 h⁻¹, and NH₃/NO = 0.9, GHSV 240,000 h⁻¹. (Gas compositions in Experimental section).

2.1. Physical Characterization

Figure 2 shows the XRD patterns of the catalysts A and B as well as of the TiO₂ support and WO₃/TiO₂ material (denoted as TiW). All of them were made in this study. Among the TiO₂ support, TiW, catalysts A, B, C, and D (the XRD profiles of catalysts C and D were not given here), there are no differences in the shape and position of the diffraction peaks except for the strength. The obtained diffraction patterns for all the samples comply with those of the TiO₂ anatase phase. No visible tungsten and vanadium oxides can be observed. Because the concentrations of tungsten and vanadium oxides were too low or well dispersed, for example, as monolayer species which are undetectable by XRD on the surface of TiO₂ [35]. The full width at half-maximum (FWHM) of the characteristic peak (with the highest intensity) for the catalyst B (0.22) is smaller than that of the catalyst A (0.47), meaning that the grain size of anatase TiO₂ crystal particles on catalyst B were larger than on catalyst A.

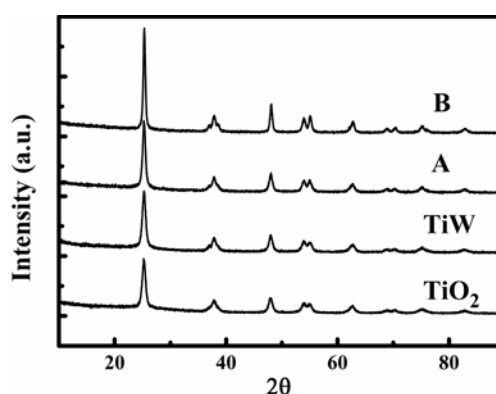


Figure 2. X-ray diffraction (XRD) profiles of catalysts A and B and major materials adopted in this study.

Table 1 summarizes the BET surface areas, pore volumes, and pore sizes of the catalysts A and B, TiW and TiO₂ support. A significant loss of surface area occurred upon the addition of V₂O₅ and WO₃ into the catalyst samples, possible due to dispersion of such added species into the pores

of TiO₂ [36]. In Table 1, the specific surface area was 108 m²·g⁻¹ for TiO₂ support. After doping with tungsten and vanadium, it decreased to 85 m²·g⁻¹ and 75 m²·g⁻¹ for the catalysts A and B, respectively. Both tungsten and vanadium oxides could be dispersed onto the support to occupy some channels of TiO₂ crystallite. Meanwhile, the second calcination after impregnation of the W and V species during the catalyst preparation might also increase the grain size of TiO₂ (see Table 1). In addition, the solvothermal method also led to a bigger crystallite size of TiO₂. All of these caused lowered surface areas and smaller pore sizes of the catalysts than of the original support.

Table 1. Texture properties of the catalysts A and B and their materials.

Samples	BET Surface Area (m ² ·g ⁻¹)	Pore Volume (cm ³ ·g ⁻¹)	Average Pore Diameter (nm)	TiO ₂ Crystallite Size ^a (nm)
TiO ₂	108	0.41	14.3	14.6
TiW	95	0.39	16.1	16.1
A	85	0.27	13.0	17.8
B	75	0.31	13.4	38.3

^a TiO₂ crystallite size was calculated from X-ray diffraction (XRD) data.

Table 1 clarifies that the pore volume and average pore diameter of the catalyst B were both larger than those of the catalyst A, indicating that there are more meso, or even macro pores in the catalyst B. Especially, the catalyst B even had a pore diameter bigger than that of the original TiO₂ support. Combining with the lowest surface area and relatively higher pore volume of this catalyst, we can suggest that in the preparation of the catalyst B both V and W oxides would mainly exist on micro channels causing more meso and macro pores to remain, indicating deep dispersion of such active metal species onto the TiO₂ support. Compared to this, the dispersion of V and W species for the catalyst A would be more onto the meso or macro pores of the TiO₂ support, having few meso and macro pores in this catalyst. Essentially, the results demonstrate the great influence of the catalyst preparation method on the catalyst pore and surface characteristics due to, for example, the difference in solvent and precursors. The method for making the catalyst B, which was newly devised in this study and uses toluene as solvent and VO(acac)₂ precursor, delivered a better dispersion of the V and W species on TiO₂ than the conventional aqueous impregnation method using ammonium metavanadate precursor.

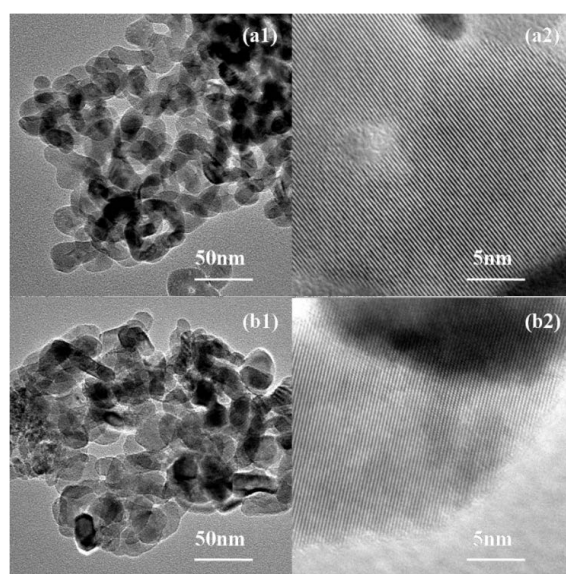


Figure 3. Transmission electron microscopy (TEM) images at different magnifications of catalysts (a) A; and (b) B.

Figure 3 shows the TEM images for the catalysts A and B at different magnifications. The surface features in Figure 3a1,b1 reveal that the catalysts A and B had obviously spherical primary particles with average particle sizes of 18 nm and 38 nm, respectively. The high-resolution images (HRTEM) in Figure 3a2,b2 further shows that the catalysts were single crystals with an average space of 0.2 nm between the aligned crystal lattice. This shows also the anatase phase of TiO_2 , as identified by XRD analysis in Figure 2. It suggests that for the catalysts A and B the oxides of tungsten and vanadium, which are the active metallic oxides of the catalysts, were highly dispersed into the lattice structure of TiO_2 to closely interact with the TiO_2 support.

2.2. Performance for SCR of NO

Figure 4a shows the realized NO conversions for simulated flue gas without SO_2 and water vapor at different reaction temperatures over the self-made catalysts A and B, TiO_2 and WO_3/TiO_2 (denoted as TiW). On raising the temperature the NO conversion first increased and then remained constant until finally turning to decrease. This variation tendency is common for SCR catalysts for denitration, but we can see that the temperature window enabling the steady NO conversion was 250–400 °C and 200–400 °C for the catalysts A and B, respectively. This means that the catalyst B had the better low-temperature activity. There was almost no NO reduction over pure TiO_2 . The NO conversion over TiW was about 75% when the temperature was higher than 350 °C. However, the N_2O concentration in the effluent gas shown in Figure 4b reached 73 ppm at such a temperature for TiW indicating its high oxidation to NH_3 or bad N_2 selectivity for SCR of NO. Consequently, the dispersion of V onto WO_3/TiO_2 is critical to achieve the activity of the catalyst for SCR of NO.

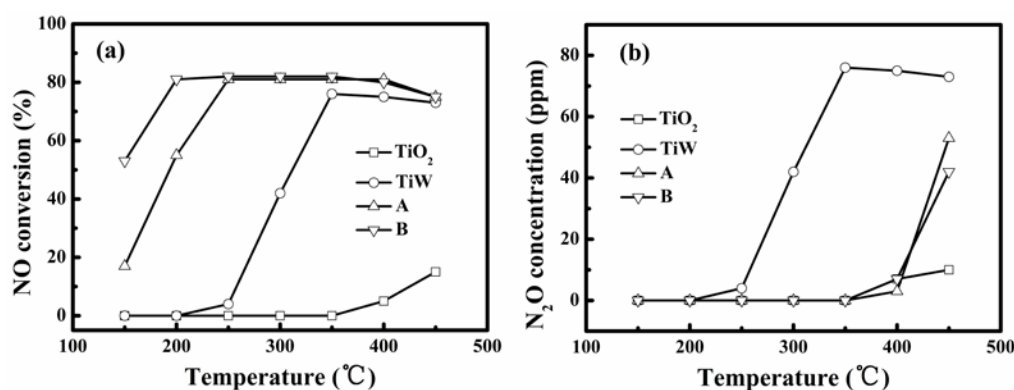


Figure 4. Evaluation for selective catalytic reduction (SCR) of NO at different temperatures over different catalysts: (a) NO conversion and (b) N_2O concentration in reacted gas (without SO_2 and water vapor in simulated flue gas and gas conditions in Experimental section).

The steady NO conversion for the catalysts A and B were similar and reached a value almost equal to the NH_3/NO molar ratio of 0.8. At 150 °C and 200 °C, the NO conversions over catalyst B were 55% and 81%, respectively. These were obviously higher than those of 18% and 56%, realized by catalyst A. Figure 4b shows further that below 400 °C there was no obvious formation of N_2O for both the catalysts. All of this shows that the prepared catalysts A and B both allowed good selectivity in SCR of NO with NH_3 to form N_2 at temperatures below 400 °C. The suitable activity temperature windows are respectively 250–400 °C and 200–400 °C for the catalysts A and B. This proves that the method of liquid-phase impregnation adopted in this study can lead to good low-temperature activity. It is related to the high-degree of dispersion of V and W oxides on the TiO_2 support realized by the liquid-phase impregnation. Furthermore, the result proves that the vanadium precursors also affect low-temperature activity. The use of $\text{VO}(\text{acac})_2$ via impregnation in toluene enabled the lowest activity temperature of 200 °C for the flue gas without presence of SO_2 and water vapor.

Below 300 °C, the poisoning of SO₂ and water vapor in the SCR of NO is usually serious because of their adsorption on the catalytic sites in competition with NH₃ and NO and the easy formation of NH₄HSO₄ that hardly decomposes at such temperatures [37]. Figure 5 shows the results from testing the activity stability of the catalysts A and B at 200–450 °C for SCR of NO from flue gas containing 350 ppm SO₂ and 10 vol. % water vapor. For comparison, a test over catalyst B was also conducted for the simulated flue gas without SO₂ and water vapor, as is shown by the data of the dotted line in Figure 5a. For all the tests, the GHSV was kept at 40,000 h⁻¹ and NH₃/NO was at 0.8 to indicate that the results shown below are for such specified conditions.

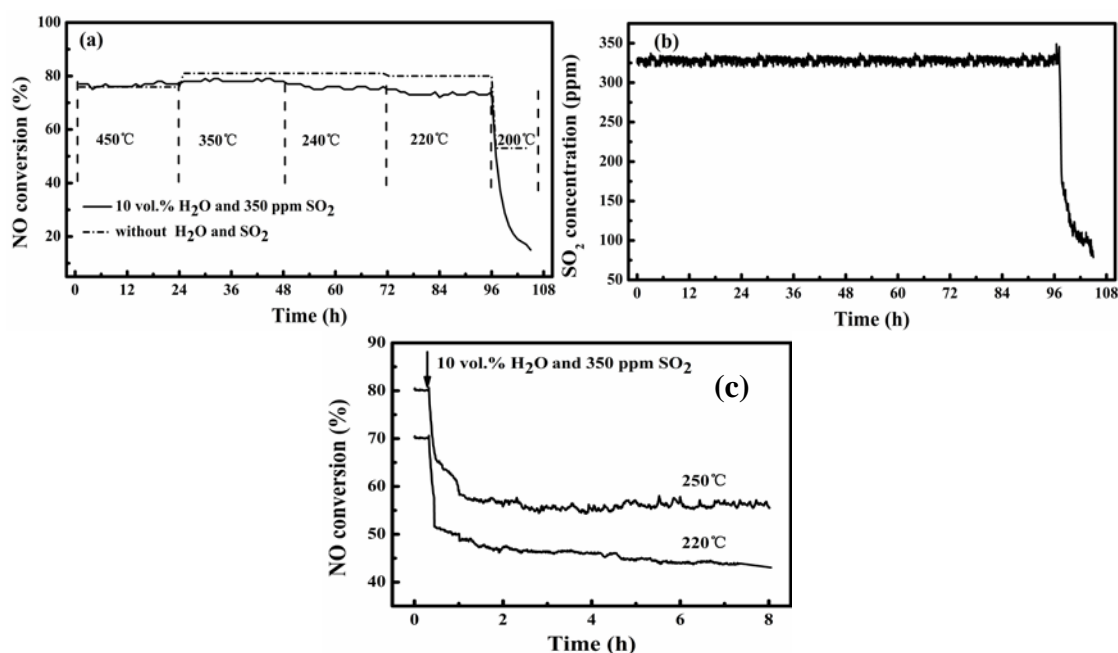


Figure 5. Stability of catalysts A and B for SCR of NO at 200–450 °C in flue gas with SO₂ and water vapor: (a) NO conversion over catalyst B in 108-h test at varied temperatures; (b) SO₂ concentration at reactor exit corresponding to (a); (c) NO conversion over catalyst A at 220 °C and 250 °C (see gas conditions in the Experimental section).

Over the catalyst B, Figure 5a shows that its activity was stable at temperatures of 220–450 °C for both the tested gas conditions (with and without SO₂ and H₂O). Except for the test at 450 °C where the NO conversion was about 76% for both gases, the presence of SO₂ and H₂O in the flue gas slightly decreased the realized NO conversion. The decrease was below 10%, but it was more obvious at the lower reaction temperature. Decreasing the temperature from 450 °C to 220 °C only slightly lowered the NO conversion, from about 80% to about 72% even for the case with SO₂ and water vapor in the flue gas. Corresponding to this, the simultaneously monitored SO₂ concentration of the effluent gas from the reactor was constantly about 330 ppm at 220–450 °C but quickly decreased with time for the test at 200 °C (shown in Figure 5b). The latter just corresponded to a rapid decrease in the NO conversion with the progress of the reaction. Figure 5a shows further that without SO₂ and H₂O in the flue gas there was a final steady NO conversion of about 52%, whereas the presence of SO₂ and H₂O caused the NO conversion to sharply decrease to below 20% in 6 h to indicate complete deactivation of the catalyst. The corresponding decrease of effluent SO₂ concentration was from 330 ppm to below 100 ppm in 6 h.

The preceding results justify the potential application of the catalyst B for denitration from flue gases having temperatures above 220 °C. Meanwhile, Figure 5c shows that the catalyst A prepared in this work is also difficult to function at 220 °C and 250 °C for flue gases containing SO₂ and H₂O. While it cannot give a steady NO removal at 220 °C, the possibly steady NO removal shown for 250 °C

is about 25 percentage points lower (80% to 55%) than that for the case without SO₂ and water vapor in the flue gas. This shows that the V impregnation through VO(acac)₂ in toluene really granted the catalyst a better low-temperature activity and stability.

Figure 6 shows the FT-IR spectra of fresh and spent catalyst B after the stability tests shown in Figure 5a. There was no obvious difference in the spectra for the fresh and spent catalyst B after 110-h reaction in flue gas without SO₂ and water vapor (dotted line in Figure 5a). The presence of SO₂ and H₂O in the flue gas caused the FT-IR spectrum of the spent catalyst to have some new bands at 1042 cm⁻¹, 1140 cm⁻¹, 1409 cm⁻¹, and 3173 cm⁻¹, respectively. The bands at 1042 cm⁻¹ and 1140 cm⁻¹ are associated with SO₄²⁻ species, and those at 1409 cm⁻¹ and 3173 cm⁻¹ are due to NH₄⁺ species. Furthermore, the band at 1409 cm⁻¹ represents the asymmetric bending vibrations of NH₄⁺ [38], while that at 3173 cm⁻¹ indicates the NH stretching [39].

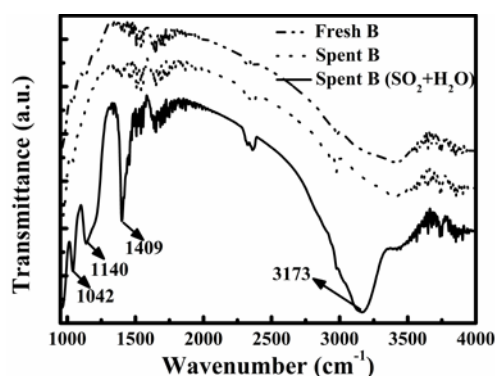


Figure 6. FT-IR spectra of fresh and spent catalyst B after tests in different simulated flue gases.

Table 2 shows the weight losses at 200–600 °C from TG analysis of spent catalyst after testing SCR of NO at 220 °C for 24 and 48 h in flue gas containing SO₂ and water vapor (conditions being the same as stated in the Experimental section). The weight loss of the spent catalyst A tested for 24 h was 2.7% and it increased on prolonging the testing time to reach 5.8% after a 48-h test. In comparison, the catalyst B had much lower weight losses of 1.3% for 24-h test and 1.5% for 48-h test, respectively. All of these justify the formation of (NH₄)₂SO₄ or NH₄HSO₄ in the NH₃-SCR reactions for flue gas containing SO₂ and water vapor (H₂O), which in turn deposit on the active sites to deactivate the catalyst for SCR of NO [10]. Nonetheless, at high temperatures such as over 300 °C, in the SCR of NO over commercial SCR catalysts the formed ammonium sulfites or sulfates can be decomposed to remove their inhibition on catalytic activity. To have steady catalytic activity, there must be a dynamic balance between the formation and decomposition of ammonium sulfite or sulfate. Thus, for catalyst B, such a dynamic balance can be built at temperatures as low as 220 °C, meaning that this catalyst would facilitate the decomposition of ammonium sulfite or sulfate at the low temperatures of 220–300 °C so that it can work stably at such low temperatures, as is shown in Figure 5a. Nonetheless, more fundamental studies, as worthwhile future work, are needed to justify the facilitated decomposition of ammonium sulfite or sulfate over catalyst B.

Table 2. Weight loss of thermogravimetric (TG) analysis at 200–600 °C for spent catalysts after SCR of NO in gas containing SO₂ and water vapor.

Catalysts	Reacted for 24 h (wt. %)	Reacted for 48 h (wt. %)
A	2.7	5.8
B	1.3	1.5

2.3. Further Justification

Figure 7 compares the NH₃-TPD profiles of the catalysts A and B. The NH₃ desorption occurred at temperatures above 100 °C for both catalysts but it was not obvious for TiO₂ until 800 °C, the highest tested temperature. Thus, there were very few acidic sites on TiO₂, although it had a high surface area of about 108 m²·g⁻¹. There are two NH₃ desorption peaks demarcated at about 300 °C for catalyst A, while catalyst B showed one major NH₃ desorption peak at 175 °C and another shoulder peak starting from 250 °C. These peaks obviously show the existence of acidic sites on the catalysts, and catalyst B had more acidic sites at a low temperature of about 175 °C leading to higher NH₃ desorption. On further noting that over TiO₂ there was no obvious NO conversion until 400 °C and catalyst B enabled a stoichiometric NO removal of 81% at 200 °C, we can conclude that the activity of a catalyst for SCR of flue gas NO is closely related to the acidic sites on the catalyst surface, and more NH₃ adsorption could improve the SCR reaction rate.

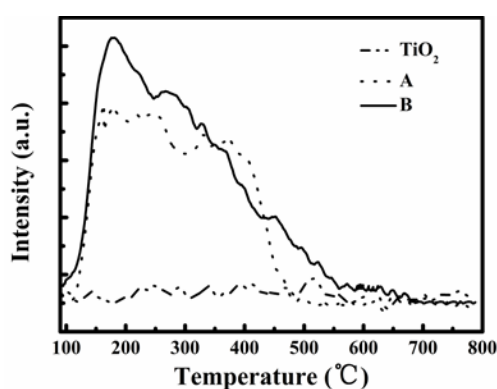


Figure 7. NH₃-TPD profiles for catalysts A and B and TiO₂ support.

Figure 8 presents the XPS spectra of V, O, and Ti given by XPS analyses for the catalysts A and B and also the self-made TiO₂ and WO₃/TiO₂ (TiW). A few ratios of surface atomic concentrations are summarized in Table 2 for elements V, O, and Ti. The Ti 2p XPS spectra in Figure 8a consists of double peaks (Ti 2p_{1/2} and 2p_{3/2}). For TiO₂, the binding energies of these peaks were 464.5 and 458.6 eV, respectively. This indicates that Ti existed in the Ti⁴⁺ state on the TiO₂ support. With the presence of V and W, the binding energies for such peaks moved to the right side with slightly lower values. Thus, the impregnated V and W would have strong interactions with the TiO₂ support. Especially, such a kind of interaction on catalyst B is stronger than on catalyst A because the binding energies of the two peaks are lowest for catalyst B.

The O 1s peaks in Figure 8b could be fitted into two peaks referring to the lattice oxygen (denoted as O_α) at 529.8–530.4 eV and the chemisorbed oxygen (denoted as O_β) at 531.1–531.9 eV, as shown by the two dotted fitting curves. The peaks of O 1s are shifted to the side with lower binding energy values, and the concentrations of chemisorbed oxygen O_β gradually increased according to the order of TiO₂, TiW, catalyst A, and catalyst B. The ratio of O_β/(O_α + O_β) calculated from the areas of the two fractionate peaks was 0.31 for the catalyst B, bigger than those for the others. Jing *et al.* [40] reported that chemisorbed oxygen O_β is the most active oxygen and plays an important role in NH₃-SCR of NO. Because the chemisorbed oxygen is more active in oxidation, the high O_β ratio in catalyst B would accelerate the oxidation of NO during SCR reactions.

Figure 8c displays the XPS spectra for V 2p of the catalysts A and B. There are two cross peaks to represent the V 2p_{1/2} and V 2p_{3/2}, respectively. Each of them can be further separated into two fractionating peaks to analyze the valence interchange between V⁴⁺ and V⁵⁺. A similar result should be obtained by treating the peak of either V 2p_{1/2} or V 2p_{3/2}, and here we take the latter. The fractionate peaks appearing at 515.8 and 516.9 eV can be ascribed to V⁴⁺ 2p_{3/2} and V⁵⁺ 2p_{3/2}, respectively. Thus, the V species were in V⁴⁺ and V⁵⁺ states on the catalysts A and B. The surface atomic ratio

of $V^{4+}/(V^{4+} + V^{5+})$ was 0.64 for catalyst B (the area ratio of the two fractionated peaks), higher than that for catalyst A (0.41). Zhang *et al.* [41] reported that the reduction species V^{4+} and V^{3+} were the active sites for the formation of superoxide ions that enhance activity at low temperatures. The transformation between V^{4+} and V^{5+} contributes to the catalytic activity for NH_3 -SCR reactions [42]. Nonetheless, the catalysts A and B had very different ratios of peak areas between V and Ti, as shown in Table 3 via the V/Ti ratio; 0.03 and 0.09 for catalysts A and B, respectively. Both a high ratio of $V^{4+}/(V^{4+} + V^{5+})$ and a high atomic concentration of vanadium (*i.e.*, a high V/Ti ratio) on the catalyst surface are critical for the catalytic activity of a catalyst [41–43]. Furthermore, the higher surface atomic concentration of vanadium indicates more active sites on the catalyst surface, which in turn increases the activity and stability of the catalyst.

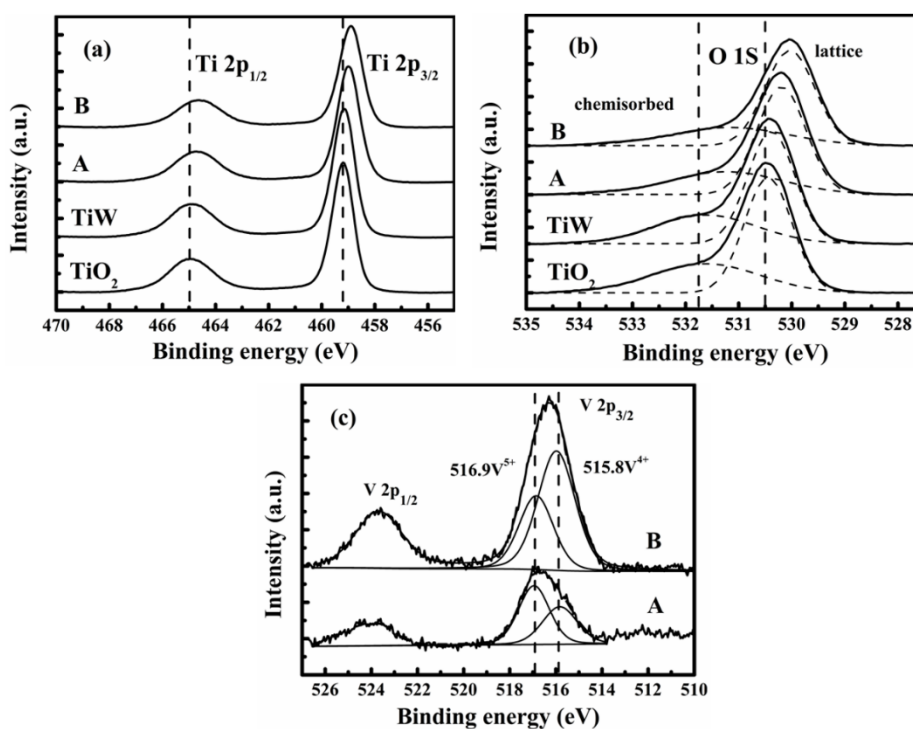


Figure 8. X-ray photoelectron spectrometry (XPS) spectra of (a) Ti 2p; (b) O 1s; and (c) V 2p for two catalysts and self-made TiO_2 support and WO_3/TiO_2 .

Table 3. Surface atomic concentration from XPS spectra in Figure 7.

Samples	Surface Atomic Concentration		
	V/Ti	$O_{\alpha}/(O_{\alpha} + O_{\beta})$	$V^{4+}/(V^{4+} + V^{5+})$
TiO_2	-	0.37	-
A	0.03	0.33	0.41
B	0.09	0.31	0.64

Figure 9 shows the H_2 -TPR profiles for all the tested samples. For TiO_2 there was almost no reduction peak. Dispersing WO_3 onto a TiO_2 support caused a strong peak at $583^\circ C$ and two weak peaks centered around $660^\circ C$ and $743^\circ C$ for WO_3/TiO_2 (TiW). Reiche *et al.* [44] reported two peaks around $467^\circ C$ and $782^\circ C$, which were attributed to reduction of W^{6+} species. Here we also consider that all three peaks of TiW are attributed to the reduction of W^{6+} species. When W and V were further introduced into the TiO_2 support, three peaks at $544^\circ C$, $660^\circ C$, and $824^\circ C$ were found for catalyst A. According to literature studies [4,44,45], the peak at $544^\circ C$ is indicative of the well-dispersed V species, while the others are suggested to be reduction of W^{6+} species. For catalyst B, three peaks appeared

at about 460 °C, 632 °C, and 825 °C, respectively. The peak at 460 °C, which moved to a much lower temperature compared to 544 °C for the catalyst A, was attributed to the reduction of V species. Comparing with TiW, one can see that the H₂ consumption profile due to the V species is shown by a broad peak with a similar starting temperature of about 350 °C but different finishing temperatures for catalysts A and B. While the peak was complete at about 620 °C for catalyst A, the temperature was about 580 °C for catalyst B. The latter indicates that the vanadium species on catalyst B are easier to reduce, implying a better dispersion of the V species and thus a better low-temperature activity.

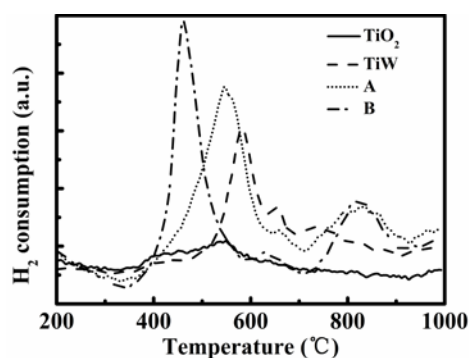


Figure 9. H₂-TPR (temperature-programmed reduction) curves of the tested two catalysts A and B, TiO₂ support and WO₃/TiO₂.

The lower reduction temperature of the V species for catalyst B shown in Figure 9 suggests that its V species is easier to be reduced by H₂. This indicates that the V species have stronger interaction with the TiO₂ support and better dispersion over the surface of the catalyst when using VO(acac)₂ as the vanadium precursor. Corresponding to the lower reduction temperature of the V species, catalyst B enabled a higher SCR activity as shown above. Literature studies have widely recognized the higher reducibility of the SCR catalyst, that the higher catalyst activity is for NH₃-SCR at the reduction temperature [46].

As a consequence, the illustrations from Figure 7 to Figure 9, not only justify the better low-temperature activity and stability of catalyst B prepared by following a newly proposed method using VO(acac)₂ precursor in toluene solvent, but verify also that the redox of the active component or the interaction between the active component and TiO₂ support plays an important role on the activity of a catalyst for NH₃-SCR of NO.

3. Experimental Section

3.1. Catalyst Preparation and Evaluation

The TiO₂ support was prepared by the atmospheric hydrolysis method. First, a titanyl sulfate solution was prepared by stirring 100 g titanyl sulfate (TiOSO₄, Jingchun, Shanghai, China) mixed with 400 mL of deionized water in a round-bottom flask at 40 °C for 6 h. In turn, urea (CO(NH₂)₂, Sinopharm, Shanghai, China) was added to the solution, and the solution was stirred at 110 °C for 10 h. Then, the sample was filtered and washed several times using deionized water until the pH value of the waste solution became about pH 7. Finally, the TiO₂ support obtained as the filter cake was dried at 110 °C for 10 h and calcined at 500 °C for 4 h.

The WO₃/TiO₂ material (denoted as TiW) was prepared by the wet impregnation method. The ammonium metatungstate and self-made TiO₂ were mixed into deionized water with stirring at 60 °C ensured by a water bath until the solution became a paste. Then the paste was dried at 110 °C for 10 h and calcined at 500 °C for 4 h.

The tested catalysts A and D were prepared following the usual impregnation method using ammonium metavanadate (NH₄VO₃, Sinopharm, Shanghai, China) and vanadyl acetylacetonate

(VO(acac)₂, Sinopharm, Shanghai, China) as the vanadium precursors, respectively. The catalysts B and C were made according to the solvothermal method using VO(acac)₂ and NH₄VO₃ as the precursors, respectively. NH₄VO₃ was dissolved in deionized water and VO(acac)₂ in solvent toluene. All the catalysts were made to have the same composition of metal oxides, 2 wt. % V₂O₅, 5 wt. % WO₃ and balanced TiO₂. The formed meshes were converted into the tested catalysts, in succession, through filtration, desiccation at 110 °C in air for 10 h, and calcination at 500 °C for 4 h in an air oven. Finally, the catalyst samples were smashed and sieved through 50–100 meshes for activity evaluation. All the used materials and solvents for catalyst preparation and experiments were commercially bought.

Their performances for SCR of NO were evaluated in a fixed-bed quartz reactor electrically heated. The typical reaction conditions were 1.5 g smashed catalyst sample in a 1000 mL·min⁻¹ flow of N₂-balanced simulated flue gas consisting of 600 ppm NO, 480 ppm NH₃, 5 vol. % O₂, 350 ppm SO₂ (when used) and 10 vol. % H₂O (vapor when used), giving a gas hourly space velocity (GHSV) of 40,000 h⁻¹. The NH₃/NO molar ratio was fixed at 0.8, and mass flow meters monitored the flows of the simulated flue gas and N₂-base 8 vol. % NH₃. At high GHSV, the diffusion effect is weak so that the reaction is more subject to kinetic control. A GHSV 240,000 h⁻¹ was obtained by increasing the gas flow rate to 6000 mL·min⁻¹, and the NH₃/NO molar ratio was 0.9. The water vapor was generated inside the reactor by injecting a well-defined tiny water-flow into the reactor above the catalyst bed. Thus, the vaporized water was mixed with the dry gas inside the reactor to form a simulated vapor-containing flue gas. The temperature of the reactor could be program-controlled or constantly kept at a specified value. The concentrations of all components in the fed and reacted gas were continually monitored using an ABB-AO2020 on-line flue gas analyzer (ABB, Frankfurt, Germany). The realized conversion of NO was calculated with the following equation:

$$\text{NO}_{\text{conversion}} = \frac{C_{\text{NO}}^{\text{in}} - C_{\text{NO}}^{\text{out}}}{C_{\text{NO}}^{\text{in}}} \times 100\% \quad (1)$$

where $C_{\text{NO}}^{\text{in}}$ and $C_{\text{NO}}^{\text{out}}$ refer to the NO concentrations of dry gas at the reactor inlet and outlet, respectively. This means that any change in gas flow rate through the DeNO_x reactions was neglected.

3.2. Catalyst Characterization

X-ray diffraction (XRD) analysis was carried out on a Rigaku Rotaflex D/Max-RB system (Rigaku Rotaflex, Tokyo, Japan) with Cu-K α radiation at $\lambda = 0.15418$ nm. A catalyst sample was loaded on a sample holder at a depth of about 1 mm. Scanning was taken over a 2θ rang of 10–90° at a speed of 10° min⁻¹. The average crystallite size was calculated by Scherer's formula,

$$D = \frac{K\lambda}{\beta \cos\theta} \quad (2)$$

where D is the average crystallite size; K is a constant (0.94), λ is the wavelength of the X-ray radiation (0.15418 nm), θ and β refer to the diffraction angle and the full width at half-maximum (FWHM) of the diffraction peak, respectively.

The specific surface area, pore volume and pore size were obtained at -196 °C from a Quantachrome NOVA Automated Gas sorption system (Quantachrome, FL, USA). The Brunauer-Emmett-Teller (BET) specific surface area was calculated from the nitrogen adsorption-desorption isotherms. The sample for this test was degassed in vacuum at 300 °C for 24 h prior to measurement of the surface area and pore size distribution.

The images of transmission electron microscopy (TEM) and high resolution TEM (HRTEM) were obtained using a JEM-2100 of JEOL electron microscope (JEOL, Tokyo, Japan) at an accelerating voltage of 200 kV. The NH₃ temperature-programmed desorption (NH₃-TPD) experiments were carried out in a flow of He (140 mL·min⁻¹) over 0.1 g catalyst in the quartz U-tube reactor of the analyzer (Chem-BET pulsar TPR/TPD, Quantachrome, FL, USA). The catalyst sample was pretreated at 300 °C for 1 h in a

flow of He ($140 \text{ mL} \cdot \text{min}^{-1}$) to remove impurities, followed by cooling to $80 \text{ }^\circ\text{C}$. After pretreatment, the catalyst was treated in a stream of He-base gas with 8 vol. % NH_3 at $80 \text{ }^\circ\text{C}$ for 1 h. Ammonia (NH_3) was switched off when the catalyst was saturated, and then He was fed to purge the reactor for 2 h to remove the excessive NH_3 or weakly adsorbed NH_3 . Finally, the TPD experiment was performed at a temperature-rise rate of $5 \text{ }^\circ\text{C} \cdot \text{min}^{-1}$ by raising the sample temperature to $800 \text{ }^\circ\text{C}$. The gas-phase concentrations of all components were continually monitored using a mass spectrometer (Proline Mass Spectrometer, Ametek, Pittsburgh, PA, USA).

The temperature-programmed reduction (TPR) test was performed in a quartz U-tube reactor using approximately 100 mg of sample for each test in the same instrument as for the TPD test. The sample for measurement was pretreated at $300 \text{ }^\circ\text{C}$ for 2.5 h in a He flow. The temperature was increased from 80 to $1000 \text{ }^\circ\text{C}$ at a rate of $10 \text{ }^\circ\text{C} \cdot \text{min}^{-1}$, and the consumed H_2 in the process of temperature rise was continuously monitored on-line with process mass spectrometry (Proline Mass Spectrometer, Ametek, Pittsburgh, PA, USA).

An X-ray photoelectron spectrometer (XPS) was used to analyze the surface atomic concentration on the tested samples. The analysis was carried out on an ESCALAB 250Xi electron spectrometer (Thermo, Sussex, UK) using 100 W Al $K\alpha$ radiation ($h\nu = 1486.6 \text{ eV}$). In advance, the catalyst sample was put into the sample holder and degassed overnight at room temperature at a pressure of 10^{-9} mbar. The reported binding energy values were all corrected by referring to the binding energy of C 1s, that is 284.8 eV . For all catalyst samples in this study which did not contain carbon, the C 1s signal in the XPS spectra was from their adventitious carbon. In addition, the presented spectra were smoothed by subtracting a nonlinear background.

The FT-IR spectra were obtained using a Bruker Vector FTIR spectrometer (Bruker, Karlsruhe, Germany) with KBr-pressed disks. Thermogravimetric (TG) analysis was carried out on a Seiko TG analyzer (Seiko, Tokyo, Japan) coupled with a process mass spectrometer (Proline Mass Spectrometer, Ametek, Pittsburgh, PA, USA) to monitor the gas composition. The temperature of the TG was raised from room temperature to $1000 \text{ }^\circ\text{C}$ at a rate of $10 \text{ }^\circ\text{C}/\text{min}$ in an Ar flow.

4. Conclusions

The study showed that the solvothermal method using $\text{VO}(\text{acac})_2$ as vanadium precursor resulted in a NH_3 -SCR catalyst with stable performance for removing NO from flue gas containing SO_2 and water vapor at temperatures of 240 – $400 \text{ }^\circ\text{C}$, even potentially 220 – $450 \text{ }^\circ\text{C}$. In the catalyst the active components of W and V oxides were highly dispersed and exhibited strong interactions with the TiO_2 support. Through NH_3 -TPD it was revealed that the catalyst has more acidic sites to facilitate its better low-temperature activity and tolerance to the poisoning of SO_2 and H_2O in SCR of NO, in comparison with the catalyst made by incipient impregnation of ammonium metavanadate. In addition, analyzing the fresh and spent catalysts via FT-IR and TG showed that a dynamic balance between the formation and decomposition of ammonium sulfite or sulfate could be built at temperatures as low as $220 \text{ }^\circ\text{C}$ to ensure the stable activity of the catalyst at this temperature. The results of XPS and H_2 -TPR analyses further demonstrate that the newly prepared catalyst had a high $\text{V}^{4+}/(\text{V}^{4+} + \text{V}^{5+})$ ratio, a high vanadium atomic concentration on the catalyst surface, and a lower reduction temperature for its dispersed V species. These are all shown to be beneficial to the low-temperature activity for NH_3 -SCR of flue gas NO. Consequently, the catalyst made using $\text{VO}(\text{acac})_2$ precursor in toluene solvent should particularly work for SCR of NO at temperatures as low as $220 \text{ }^\circ\text{C}$. This study offers actually a new technology to produce the V_2O_5 - WO_3/TiO_2 catalyst for high-performance SCR of NO from stationary combustion and diesel vehicles over a wide working-temperature window such as 220 – $400 \text{ }^\circ\text{C}$. Also in the process of performing a pilot denitration test (2000 – $3000 \text{ nm}^3/\text{h}$) we used the monolith SCR catalyst prepared by our powder catalyst for real flue gas from a coke oven.

Acknowledgments: The work was financially supported by International Science and Technology Cooperation Program of China (2013DFA51530), and the strategic priority research program of the Chinese academy of sciences

(XDA07030300), and Japan Society for the Promotion of Science (JSPS) for the postdoctoral fellowship grant (P15758).

Author Contributions: L.G., F.G., J.Y and G.X. conceived and designed the experiments; L.G. performed the experiments; L.G., J.Y. and G.X. analyzed the data; L.G. wrote the paper and J.Y. and G.X. revised it.

Conflicts of Interest: The authors declare no conflict of interest.

References

1. Bosch, H.; Janssen, F. Catalytic reduction of nitrogen oxides: A review on the fundamentals and technology. *Catal. Today* **1988**, *2*, 369–532.
2. Deng, F.; Guo, X. Research progress on vehicle emission related health effects in china. *J. Environ. Health* **2008**, *25*, 174–176.
3. Busca, G.; Lietti, L.; Ramis, G.; Berti, F. Chemical and mechanistic aspects of the selective catalytic reduction of NO_x by ammonia over oxide catalysts: A review. *Appl. Catal. B* **1998**, *18*, 1–36. [[CrossRef](#)]
4. Reiche, M.; Ortelli, E.; Baiker, A. Vanadia grafted on TiO₂-SiO₂, TiO₂ and SiO₂ aerogels-Structural properties and catalytic behaviour in selective reduction of NO by NH₃. *Appl. Catal. B* **1999**, *23*, 187–203. [[CrossRef](#)]
5. Forzatti, P. Environmental catalysis for stationary applications. *Catal. Today* **2000**, *62*, 51–65. [[CrossRef](#)]
6. Busca, G.; Larrubia, M.A.; Arrighi, L.; Ramis, G. Catalytic abatement of NO_x: Chemical and mechanistic aspects. *Catal. Today* **2005**, *107*, 139–148. [[CrossRef](#)]
7. Zhang, H.; Wang, J.; Wang, Y.-Y. Cycle-based ammonia-coverage-ratio reference generator design for Diesel engine two-cell selective catalytic reduction systems via a fuzzy approach. *Fuel* **2015**, *159*, 76–83. [[CrossRef](#)]
8. Zhang, H.; Wang, J.; Wang, Y.-Y. Optimal Dosing and Sizing Optimization for a Ground Vehicle Diesel Engine Two-cell Selective Catalytic Reduction System. *IEEE Trans. Veh. Technol.* **2015**. [[CrossRef](#)]
9. Zhang, H.; Wang, J.; Wang, Y.-Y. Sensor reduction in diesel engine two-cell selective catalytic reduction (SCR) systems for automotive applications. *IEEE/ASME Trans. Mechatron.* **2014**, *20*, 2222–2233. [[CrossRef](#)]
10. Yu, J.; Guo, F.; Wang, Y.; Zhu, J.; Liu, Y.; Su, F.; Gao, S.; Xu, G. Sulfur poisoning resistant mesoporous Mn-base catalyst for low-temperature SCR of NO with NH₃. *Appl. Catal. B* **2010**, *95*, 160–168. [[CrossRef](#)]
11. *GB/T 17954-2007 Economical Operation of Industrial Boilers*; Standards Press of China: Beijing, China, 2007.
12. Adams, K.M.; Cavataio, J.V.; Hammerle, R.H. Lean NO_x catalysis for diesel passenger cars: Investigating effects of sulfur dioxide and space velocity. *Appl. Catal. B* **1996**, *10*, 157–181. [[CrossRef](#)]
13. Fu, M.; Ge, Y.; Wang, X.; Tan, J.; Yu, L.; Liang, B. NO_x emissions from Euro IV busses with SCR systems associated with urban, suburban and freeway driving patterns. *Sci. Total Environ.* **2013**, *452*, 222–226. [[CrossRef](#)] [[PubMed](#)]
14. Li, M.; Nie, Y.; Xu, J.; Qin, K.; Jing, X. Characters of NO_x emission from transit bus with SCR. *J. Jiangsu Univ.* **2011**, *32*, 38–42.
15. Kijlstra, W.S.; Brands, D.S.; Poels, E.K.; Blik, A. Mechanism of the selective catalytic reduction of NO by NH₃ over MnO_x/Al₂O₃. *J. Catal.* **1997**, *171*, 208–218. [[CrossRef](#)]
16. Ramis, G.; Angeles Larrubia, M. An FT-IR study of the adsorption and oxidation of N-containing compounds over Fe₂O₃/Al₂O₃ SCR catalysts. *J. Mol. Catal. A* **2004**, *215*, 161–167. [[CrossRef](#)]
17. Blanco, J.; Avila, P.; Suárez, S.; Martín, J.A.; Knapp, C. Alumina-and titania-based monolithic catalysts for low temperature selective catalytic reduction of nitrogen oxides. *Appl. Catal. B* **2000**, *28*, 235–244. [[CrossRef](#)]
18. Krishna, K.; Seijger, G.; van den Bleek, C.; Calis, H. Very active CeO₂-zeolite catalysts for NO_x reduction with NH₃. *Chem. Commun.* **2002**. [[CrossRef](#)]
19. Qi, G.; Yang, R.T.; Chang, R. MnO_x-CeO₂ mixed oxides prepared by co-precipitation for selective catalytic reduction of NO with NH₃ at low temperatures. *Appl. Catal. B* **2004**, *51*, 93–106. [[CrossRef](#)]
20. Qi, G.; Yang, R.T. Low-temperature selective catalytic reduction of NO with NH₃ over iron and manganese oxides supported on titania. *Appl. Catal. B* **2003**, *44*, 217–225. [[CrossRef](#)]
21. Qi, G.; Yang, R.T. Performance and kinetics study for low-temperature SCR of NO with NH₃ over MnO_x-CeO₂ catalyst. *J. Catal.* **2003**, *217*, 434–441. [[CrossRef](#)]
22. Segura, Y.; Chmielarz, L.; Kustrowski, P.; Cool, P.; Dziembaj, R.; Vansant, E.F. Characterisation and reactivity of vanadia-titania supported SBA-15 in the SCR of NO with ammonia. *Appl. Catal. B* **2005**, *61*, 69–78. [[CrossRef](#)]

23. Segura, Y.; Chmielarz, L.; Kustrowski, P.; Cool, P.; Dziembaj, R.; Vansant, E. Preparation and characterization of vanadium oxide deposited on thermally stable mesoporous titania. *J. Phys. Chem. B* **2006**, *110*, 948–955. [[CrossRef](#)] [[PubMed](#)]
24. Parvulescu, V.; Boghosian, S.; Parvulescu, V.; Jung, S.; Grange, P. Selective catalytic reduction of NO with NH₃ over mesoporous V₂O₅-TiO₂-SiO₂ catalysts. *J. Catal.* **2003**, *217*, 172–185. [[CrossRef](#)]
25. Baltés, M.; van der Voort, P.; Collart, O.; Vansant, E. The Adsorption of VO(acac)₂ on a mesoporous silica support by liquid phase and gas phase modification to prepare supported vanadium oxide catalysts. *J. Porous Mater.* **1998**, *5*, 317–324. [[CrossRef](#)]
26. Hakuli, A.; Kytökivi, A. Binding of chromium acetylacetonate on a silica support. *Phys. Chem. Chem. Phys.* **1999**, *1*, 1607–1613. [[CrossRef](#)]
27. Utriainen, M.; Kröger-Laukkanen, M.; Johansson, L.-S.; Niinistö, L. Studies of metallic thin film growth in an atomic layer epitaxy reactor using M(acac)₂ (M = Ni, Cu, Pt) precursors. *Appl. Surf. Sci.* **2000**, *157*, 151–158. [[CrossRef](#)]
28. Theriot, L.; Carlisle, G.; Hu, H. Oxovanadium (IV) complexes with N-salicylideneamino acids. *J. Inorg. Nucl. Chem.* **1969**, *31*, 2841–2844. [[CrossRef](#)]
29. Wang, Y.; Su, Q.; Chen, C.; Yu, M.; Han, G.; Wang, G.; Xin, K.; Lan, W.; Liu, X. Low temperature growth of vanadium pentoxide nanomaterials by chemical vapour deposition using VO(acac)₂ as precursor. *J. Phys. D* **2010**, *43*, 185102. [[CrossRef](#)]
30. Fedorova, E.; Rybakov, V.; Senyavin, V.; Anisimov, A.; Aslanov, L. Synthesis and structure of oxovanadium (IV) complexes [VO(Acac)₂] and [VO(Sal: L-alanine)(H₂O)]. *Crystallogr. Rep.* **2005**, *50*, 224–229. [[CrossRef](#)]
31. Van Der Voort, P.; Babitch, I.V.; Grobet, P.J.; Verberckmoes, A.A.; Vansant, E.F. Synthesis and characterization of supported vanadium oxides by adsorption of the acetylacetonate complex. *Faraday Trans.* **1996**, *92*, 3635–3642. [[CrossRef](#)]
32. Van der Voort, P. Preparation of supported vanadium oxide catalysts. Adsorption and Thermolysis of Vanadyl Acetylacetonate on a Silica Support. *Faraday Trans.* **1996**, *92*, 843–848. [[CrossRef](#)]
33. Economidis, N.V.; Peña, D.A.; Smirniotis, P.G. Comparison of TiO₂-based oxide catalysts for the selective catalytic reduction of NO: effect of aging the vanadium precursor solution. *Appl. Catal. B* **1999**, *23*, 123–134. [[CrossRef](#)]
34. Miller, J.M.; Lakshmi, L.J. V₂O₅ catalysts supported on Al₂O₃-SiO₂ mixed oxide: 51V, 1HMAS solid-state NMR, DRIFTS and methanol oxidation studies. *Appl. Catal. A* **2000**, *190*, 197–206. [[CrossRef](#)]
35. Ramis, G.; Busca, G.; Bregani, F. Fourier transform-infrared study of the adsorption and coadsorption of nitric oxide, nitrogen dioxide and ammonia on vanadia-titania and mechanism of selective catalytic reduction. *Appl. Catal.* **1990**, *64*, 259–278. [[CrossRef](#)]
36. Alemany, L.J.; Lietti, L.; Ferlazzo, N.; Forzatti, P.; Busca, G.; Giamello, E.; Bregani, F. Reactivity and physicochemical characterization of V₂O₅-WO₃/TiO₂ De-NO_x catalysts. *J. Catal.* **1995**, *155*, 117–130. [[CrossRef](#)]
37. Jin, R.; Liu, Y.; Wu, Z.; Wang, H.; Gu, T. Relationship between SO₂ poisoning effects and reaction temperature for selective catalytic reduction of NO over Mn-Ce/TiO₂ catalyst. *Catal. Today* **2010**, *153*, 84–89. [[CrossRef](#)]
38. Lin, S.D.; Gluhoi, A.C.; Nieuwenhuys, B.E. Ammonia oxidation over Au/MO_x/γ-Al₂O₃-activity, selectivity and FTIR measurements. *Catal. Today* **2004**, *90*, 3–14. [[CrossRef](#)]
39. Sayan, Ş.; Kantcheva, M.; Suzer, S.; Uner, D. FTIR characterization of Ru/SiO₂ catalyst for ammonia synthesis. *J. Mol. Struct.* **1999**, *480*, 241–245. [[CrossRef](#)]
40. Jing, L.; Xu, Z.; Sun, X.; Shang, J.; Cai, W. The surface properties and photocatalytic activities of ZnO ultrafine particles. *Appl. Surf. Sci.* **2001**, *180*, 308–314. [[CrossRef](#)]
41. Zhang, S.; Zhong, Q.; Zhao, W.; Li, Y. Surface characterization studies on F-doped V₂O₅/TiO₂ catalyst for NO reduction with NH₃ at low-temperature. *Chem. Eng. J.* **2014**, *253*, 207–216.
42. Zhang, S.; Li, H.; Zhong, Q. Promotional effect of F-doped V₂O₅-WO₃/TiO₂ catalyst for NH₃-SCR of NO at low-temperature. *Appl. Catal. A* **2012**, *435*, 156–162. [[CrossRef](#)]
43. Liu, Y.-M.; Cao, Y.; Yi, N.; Feng, W.-L.; Dai, W.-L.; Yan, S.-R.; He, H.-Y.; Fan, K.-N. Vanadium oxide supported on mesoporous SBA-15 as highly selective catalysts in the oxidative dehydrogenation of propane. *J. Catal.* **2004**, *224*, 417–428. [[CrossRef](#)]
44. Reiche, M.; Maciejewski, M.; Baiker, A. Characterization by temperature programmed reduction. *Catal. Today* **2000**, *56*, 347–355. [[CrossRef](#)]

45. Au, C.; Chen, K.; Ng, C. The modification of Gd_2O_3 with BaO for the oxidative coupling of methane reactions. *Appl. Catal. A* **1998**, *170*, 81–92. [[CrossRef](#)]
46. Paganini, M.C.; Dall'Acqua, L.; Giamello, E.; Lietti, L.; Forzatti, P.; Busca, G. An EPR Study of the Surface Chemistry of the V_2O_5 - WO_3 / TiO_2 Catalyst: Redox Behaviour and State of V (IV). *J. Catal.* **1997**, *166*, 195–205. [[CrossRef](#)]



© 2016 by the authors; licensee MDPI, Basel, Switzerland. This article is an open access article distributed under the terms and conditions of the Creative Commons by Attribution (CC-BY) license (<http://creativecommons.org/licenses/by/4.0/>).